

Hyperfine and Zeeman Splitting of ^{85}Rb and ^{87}Rb

Adam Green, Guillermo Acuna

agree019@ucr.edu, gacun002@ucr.edu

Department of Physics & Astronomy, University of California, Riverside, CA 92521

Abstract

In this experiment, study the hyperfine splitting and Zeeman effect for naturally occurring Rubidium using saturated absorption spectroscopy. For ^{85}Rb , we measure the splitting between the $F = 2$ and $F = 3$ states to be $3320 \text{ MHz} \pm 117 \text{ MHz}$. For ^{87}Rb , we determine the splitting between the $F = 1$ and $F = 2$ state to be $7390 \text{ MHz} \pm 117 \text{ MHz}$. We provide quantitative energy level diagrams for both isotopes of Rubidium. Further, upon the application of an external magnetic field, we measure the splitting between the hyperfine transitions. We provide an analysis of Zeeman splitting vs magnetic field strength and we determine the Landé g-factor to be $g_F = 0.307 \pm 0.0103$.

Contents

1	Introduction	1
2	Experimental Procedure	3
2.1	Optical Setup	5
3	Results and Analysis	6
3.1	Fine Structure Spectrum	7
3.2	Hyperfine Structure Spectrum	7
3.3	Zeeman Effect	9
3.4	Landé g-factor	10
4	Conclusion	11
4.1	Error	11
4.2	Extensions - Need more!	11
5	Appendix	12
5.1	Mode Hopping	12
5.2	Zeeman Splitting	13

1 Introduction

The ground states of Hydrogen and Rubidium have effectively the same electron configuration. Hydrogen consists of a single 1s electron while Rubidium consists of a closed shell plus a single 5s electron. This indicates that their spectra should share similar features. Solving the Schrödinger

equation yields energies dependent on the principal quantum number “ n ” which contains n^2 degeneracies.

These degeneracies are resolved when a number of corrective effects are included. The first is a statement that electrons are moving at relativistic speeds which affects their kinetic energy simply known as the *relativistic kinetic energy* correction. The second two only effect the s-orbital: the *Darwin Term* is the smearing out of the Coulomb interaction between the nucleus and electron due to quantum fluctuations and the *Lamb shift* arises from quantum electrodynamic interactions between the electrons and the vacuum. Finally, the spin and orbital angular momentum of the electron interact with each other giving rise to a *spin-orbit coupling* effect. Due to this coupling, the quantum numbers representing the orbital angular momentum and spin, L and z respectively, are no longer good quantum numbers and are replaced by the total angular momentum, $J = L + S$, and its projection along the z-axis, J_z . Collectively these three effects are known as the *fine structure* and are visualized in Fig. 1.

These states are denoted by “term states” in the spectroscopic notation $^{2S+1}L_J$, where L is the spectroscopic notation, S, P, D, F for the corresponding orbital angular momentum quantum numbers $L = 0, 1, 2, 3$. In this notation, the ground state of the 5s Rb electron is denoted as $^2S_{1/2}$ and the first excited state is denoted $^2P_{3/2}$.

It turns out that the fine structure is still degenerate. To resolve these degeneracies, we must account for one additional effect. If the nucleus has a magnetic moment, denoted by \vec{I} , the electron feels the magnetic field produced by the nucleus. Thus, the energy of the electron now depends on the spin orientation relative to the magnetic field produced by the nucleus, known as the *Zeeman Effect*. The additional corrections to the fine structure energy levels are known as the *hyperfine structure* corrections. If the hyperfine splitting is much less than the fine structure splitting, then the magnetic quantum number $I = |\vec{I}|$ and orbital angular momentum quantum number J are good quantum numbers. Further, the degeneracy in the fine structure is split according to total the angular momentum $F = I + J$. Note that F takes values between $\{|I - J|, |I - J + 1|, \dots, |I + J|\}$. With respect to the fine structure, the energy levels are split by:

$$E = \frac{\gamma}{2} [F(F+1) - I(I+1) - J(J+1)] \quad (1)$$

where γ is the hyperfine structure constant.

Rubidium has two naturally occurring isotopes, ^{85}Rb (72% abundance) with $I = \frac{5}{2}$, and ^{87}Rb (28% abundance) with $I = \frac{3}{2}$. A spectroscopic analysis of naturally occurring Rubidium will contain both isotopes superimposed on top of each other.

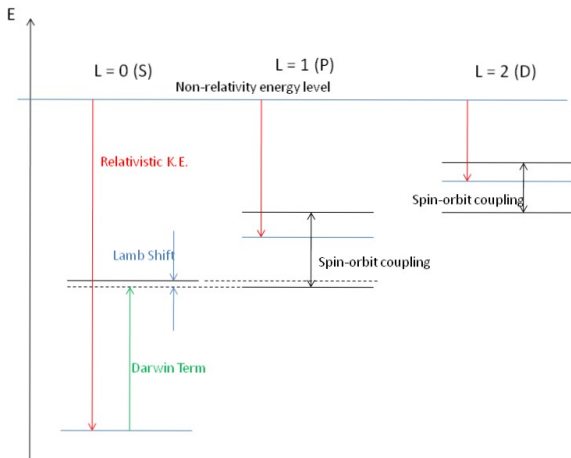


Figure 1: Qualitative energy level diagram displaying the fine structure corrections for Hydrogen

For an atom with magnetic moment μ , a magnetic field will perturb it by:

$$\Delta E = -\mu \cdot \mathbf{B} \quad (2)$$

If the magnetic field is weak, the Zeeman splitting is small compared to the hyperfine interactions. In the weak field limit, the Zeeman splitting to first order is given by:

$$\Delta E_{\text{weak}} = g_F \mu_B m_F B \quad (3)$$

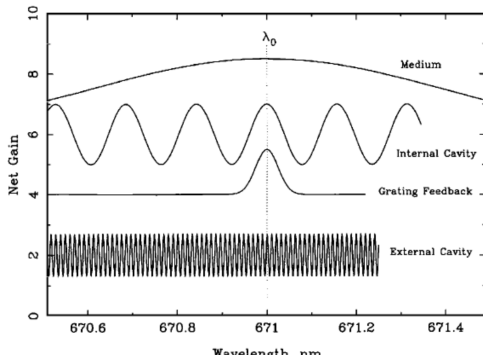
where $g_F \approx g_J \frac{F(F+1) - I(I+1) - J(J+1)}{2F(F+1)}$, g_J is the *Landé g-factor*, μ_B is the *Bhor Magneton*, and $m_F = -F, -F + 1, \dots, F$ is the quantum number for F_z . ■

2 Experimental Procedure

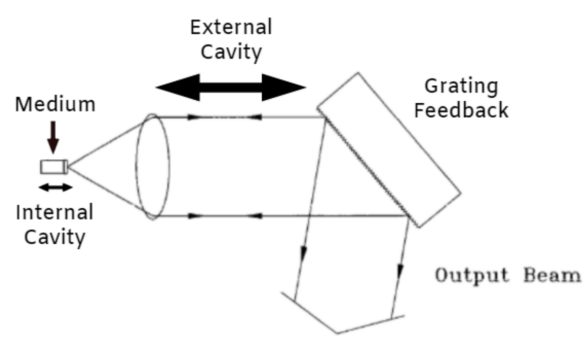
Mode Hopping

Mode hopping is an undesirable feature of diode lasers and produces very sharp, discontinuous jumps in spectral scans, see Fig. 14. The frequency of the laser beam is actually a combination of the frequencies allowed by the various parts of the laser, see Fig. 2. The parts which contribute to the frequency are 1). the material of the diode, 2). the physical size of the internal cavity in the diode, 3). the diffraction grating and 4). the separation between the collimating lens and diffraction grating called the external cavity.

Here, each of the 4 components helps to “choose” the frequency of the laser, the frequency which all components agree on. In Fig. 2a, the contribution from the medium corresponds to a wavelength range from 670 nm to 671 nm. The contribution from the grating feedback selects wavelengths in the neighborhood of 671 nm, and the contribution from the external cavity acts as the “fine tuning” to the wavelength. Mode hops are discrete jumps in the wavelength of the laser due to changes in the various contributions to the wavelength, see Fig. 15.



(a) caption



(b) caption

Figure 2: **caption**

Doppler Broadening

Doppler broadening is the broadening of a signal due to the relative velocity of the atoms interacting with the laser. For this experiment, we are sending a laser through a chamber of nat-

urally occurring Rubidium, referred to as the absorption chamber, and measuring the absorption spectrum. The velocity of the gas inside the chamber follows a Maxwellian distribution, meaning some of the molecules are moving with or against the laser. It is precisely this because of this relative motion that some of the gas molecules see the laser red-shifted, or blue-shifted onto absorption. In other words, some of the atoms in the absorption chamber which are not eligible for absorption are Doppler shifted into absorption, giving a wider range of absorbed frequencies. This “widening” of the absorption frequency is what is known as Doppler broadening.

Saturated Absorption

Saturated absorption spectroscopy reveals the hyperfine structure of Rubidium. More precisely, it resolves very fine absorption lines from a Doppler broadened signal in a two step process. To perform saturated absorption, the beam from the laser must be split into two, one weak and one strong beam. The weak beam, called the *probe* beam, is sent through the Rubidium chamber into the photodiode. The strong beam, called the *pump* beam, is aligned anti-parallel to the probe beam. The first step in saturated absorption involves the pump beam keeping the electrons in the substance perpetually excited. If the pump beam were measured, it would yield a Doppler broadened absorption spectrum just as before. Of those excited electrons, upon interacting with the probe beam, they will undergo stimulated emission. This is the second step in saturated absorption spectroscopy. This stimulated emission only occurs if the atoms see both lasers at an absorption frequency. In other words, if atoms are Doppler shifted into absorption by the pump beam, they will not undergo stimulated emission by the probe beam and thus do not contribute to the fine structure spectrum.

Crossover Resonance

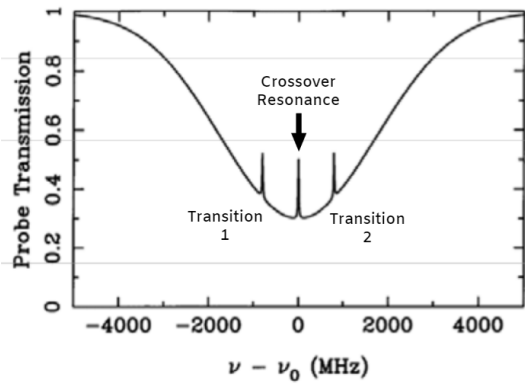


Figure 3: Saturated absorption spectrum for an atom with a single ground state and two excited states displaying a crossover resonance.

the pump or only the probe beam, and this single-beam absorption is what causes crossover resonances. Consequently, one of the distinguishing features of crossover resonances is they will always

be directly in between transitions.

Calibration

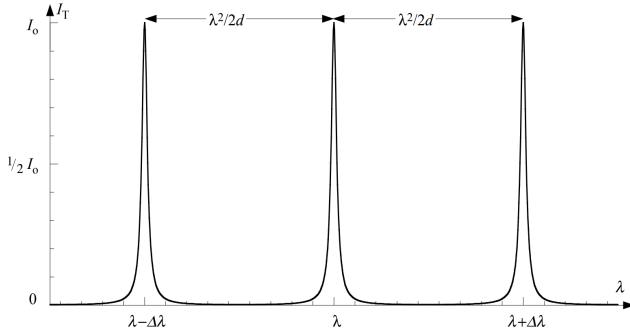
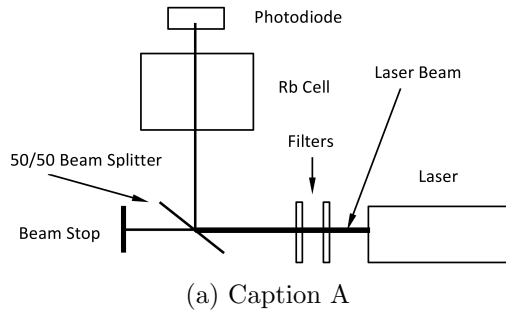


Figure 4: Representative interferometer oscilloscope trace

the length of the interferometer. A simple conversion from wavelength to frequency allows us to determine the scale of the horizontal axis on the oscilloscope in terms of laser frequency. This calibration process has already been preformed, and we quote the result of 234 MHz/ms.

2.1 Optical Setup

We begin by configuring our laser bench according to Fig. 5a and the controller according to Fig. 5. In this configuration, the beam is sent through filters to a 50/50 beam splitter and then through the chamber containing the Rubidium. The resulting spectrum contains mode hopping, as seen in Fig. 14 in the appendix. Adjusting the piezoelectric DC offset and current amplitude accordingly will eliminate this mode hopping.



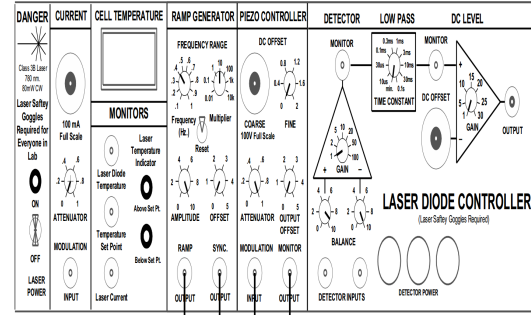
(a) Caption A

To quantify the scale of the horizontal axis on the oscilloscope, we must relate the frequency of the laser to the spacing on the oscilloscope. To do this, we use a *Fabry-Perot interferometer*. This is an optical cavity of fixed length which acts as a filter, allowing only certain frequencies to pass through. Upon measuring the transmission intensity from the interferometer, we obtain a spectrum similar to Fig. 4. Here, the spacing between each resonant peak is

$$\Delta\lambda = \frac{\lambda^2}{2d} \quad (4)$$

where λ is the frequency of the laser and d is

the length of the interferometer. A simple conversion from wavelength to frequency allows us to determine the scale of the horizontal axis on the oscilloscope in terms of laser frequency. This calibration process has already been preformed, and we quote the result of 234 MHz/ms.



(b) Caption B

Figure 5: Optical setup and controller hook ups for measurements with mode hopping.

To obtain the spectrum with the background subtracted out, we configure the optics according to Fig. 6a and the laser diode controller according to Fig. 6b. This time, the signal from photodiode 2 is subtracted from the signal from photodiode 1.

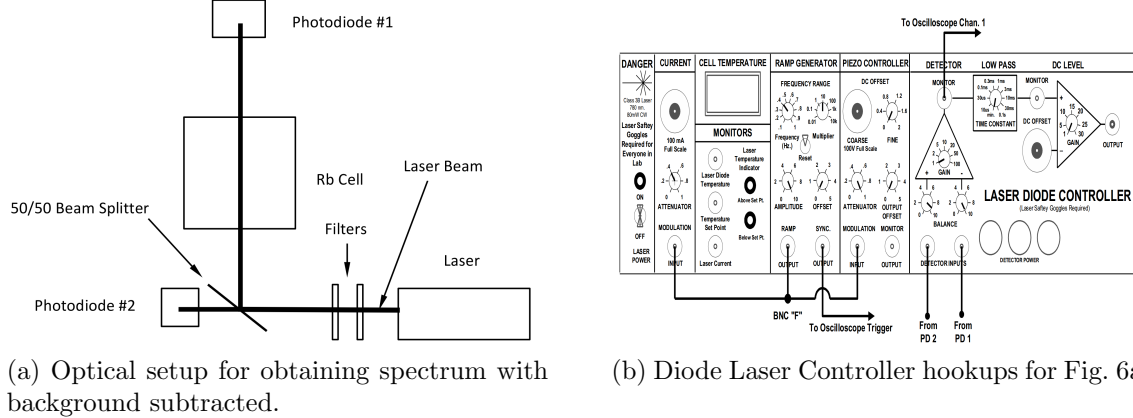


Figure 6: Laser setup and controller hookups for obtaining the spectrum with the background subtracted out

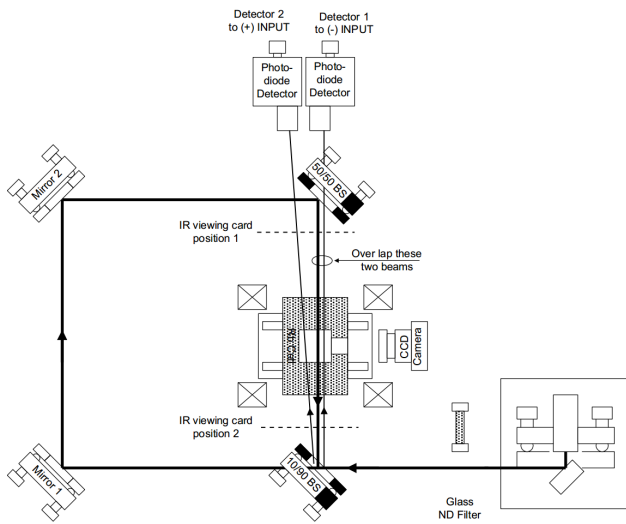


Figure 7: Optical setup for saturated absorption measurements

To obtain the hyperfine structure of the two Rubidium isotopes, we configure the laser bench according to Fig. 7. In this setup, the signal from photodiode 2 is again subtracted from photodiode 1. This time however, the signal from photodiode 1 is saturated, which reveals the hyperfine structure after the subtraction.

When aligning the beams, two considerations must be taken into account. First, it is crucial that the beams overlap as much as possible within the absorption chamber. The larger the overlap, the sharper the higher the saturated absorption peaks will appear on the oscilloscope. Second, it is important to check that after alignment, the pump beam is not being reflected off the 10/90 beam splitter, back through the absorption cell and into either photodetector. This will result in unwanted background.

3 Results and Analysis

3.1 Fine Structure Spectrum

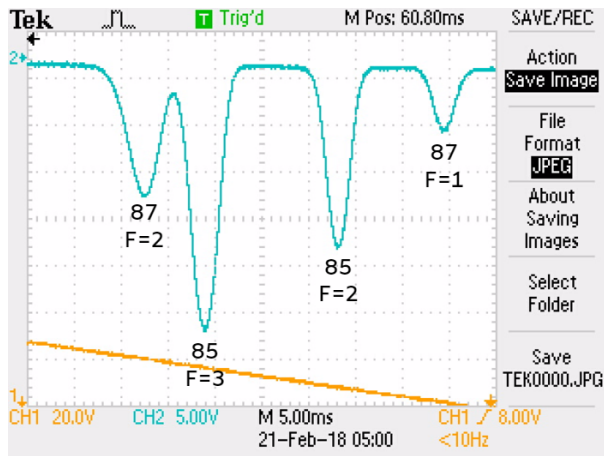


Figure 8: Annotated fine structure absorption spectrum of ^{85}Rb and ^{87}Rb

3.2 Hyperfine Structure Spectrum

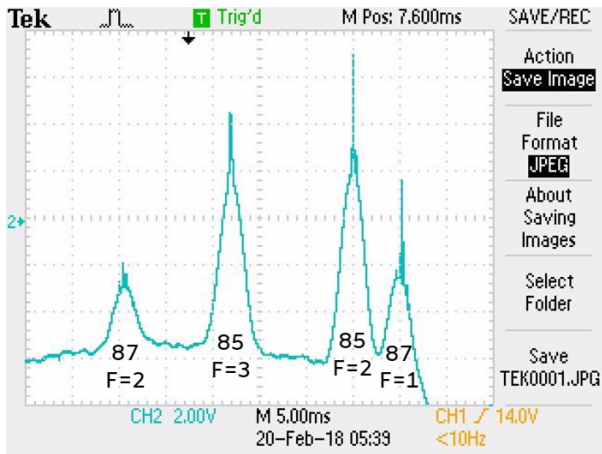


Figure 9: Hyperfine spectrum with background subtracted

After configuring the optical bench according to Fig. 6a, we measured the fine structure of the Rubidium sample. An annotated spectrum is provided below in Fig. 8. It is important to note that because the sample of Rubidium is naturally occurring, the absorption spectra of both are superimposed on each other.

After setting up the laser for saturated absorption, we can see a rough scan of the Hyperfine structure for both isotopes in Fig. 9. The widened base is due to the imperfect subtraction of the two signals and the sharp peaks are the hyperfine transitions. Fig. 10 and Fig. 11 below show annotated scans of the hyperfine transitions after zooming into each peak. It is important to note the crossover resonances which lie directly in between atomic transitions.

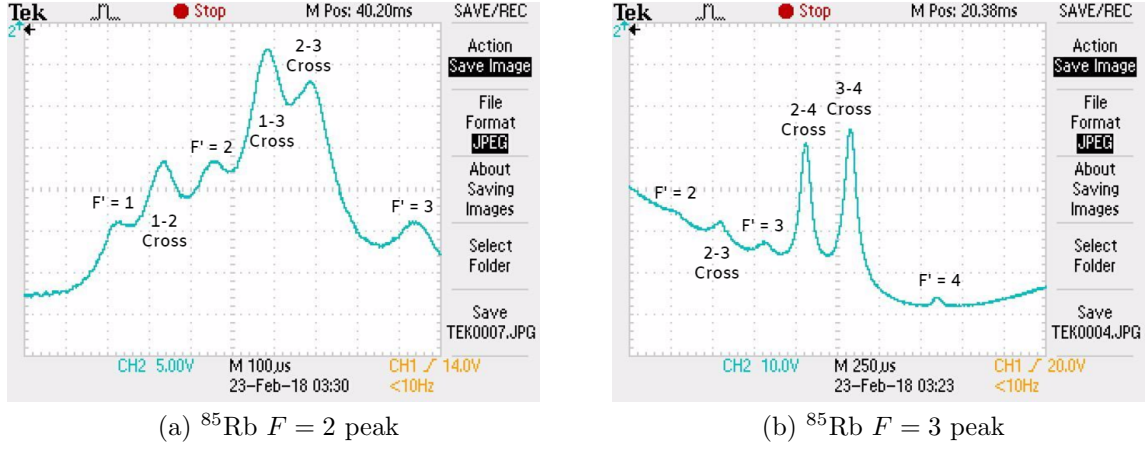


Figure 10: Hyperfine transitions of the ^{85}Rb -a transition (a) and the ^{85}Rb -b transition (b).

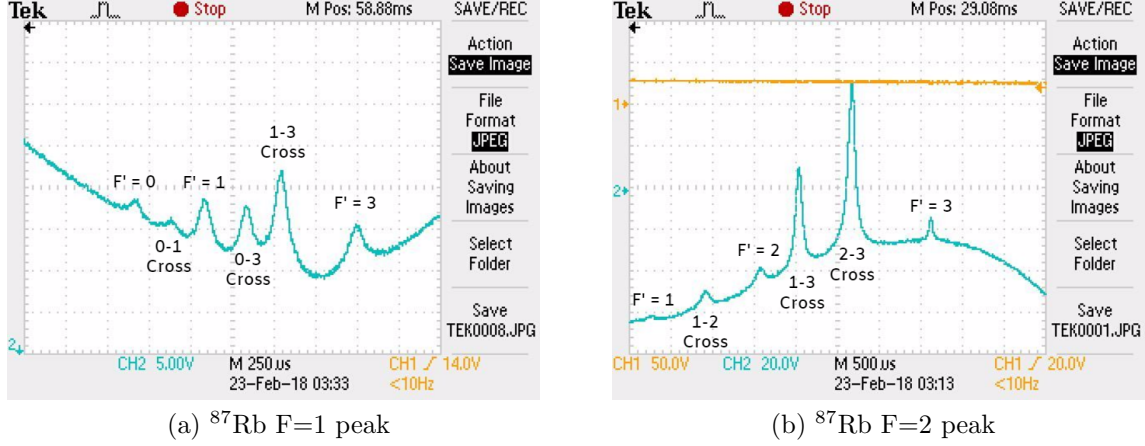
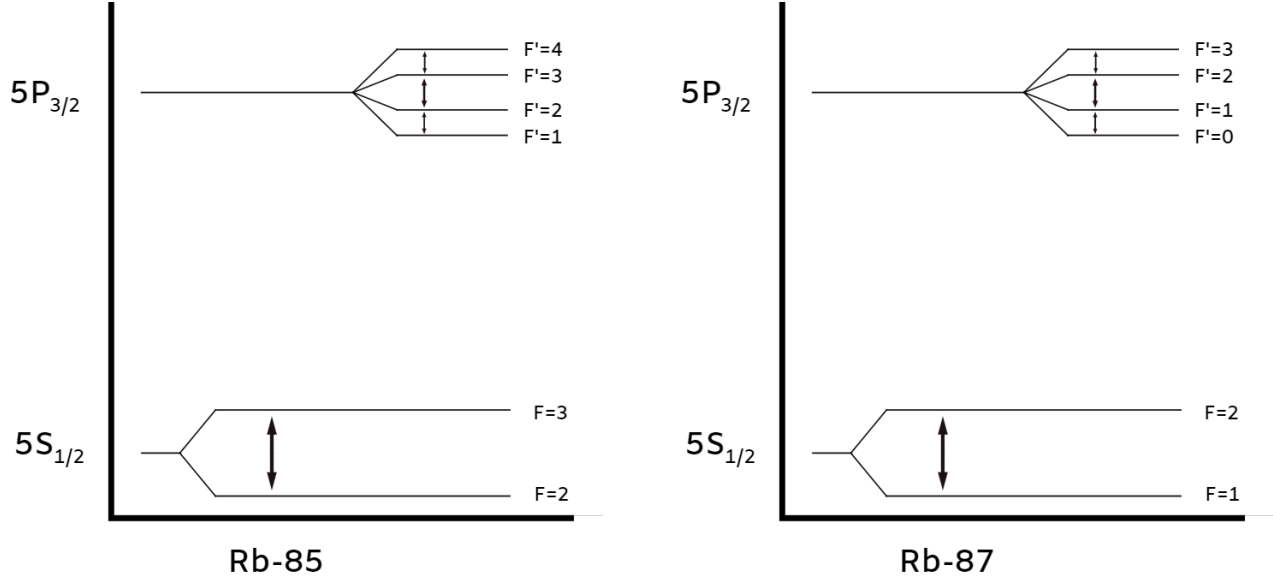


Figure 11: Hyperfine transitions of the ^{87}Rb -a transition (a) and the ^{87}Rb -b transition (b).

We provide below in Fig. 12, quantitative energy level diagrams for ^{85}Rb and ^{87}Rb . The energies of the hyperfine transitions are summarized in Tabs. 1 and 2

(a) Energy level diagram for ^{85}Rb (b) Energy level diagram for ^{87}Rb Figure 12: Energy level diagrams for ^{85}Rb and ^{87}Rb .

Transition	Frequency (MHz)	Uncertainty (MHz)
$F' = 4 \rightarrow F' = 3$	242	± 26.3
$F' = 3 \rightarrow F' = 2$	114	± 26.3
$F' = 2 \rightarrow F' = 1$	55.0	± 26.3
$F = 3 \rightarrow F = 2$	3320	± 117

Table 1: Table of transition energies for ^{85}Rb corresponding to Fig. 12a

Transition	Frequency (MHz)	Uncertainty (MHz)
$F' = 1 \rightarrow F' = 0$	94.8	± 29.3
$F' = 2 \rightarrow F' = 1$	281	± 58.5
$F' = 3 \rightarrow F' = 2$	462	± 58.5
$F = 2 \rightarrow F = 1$	7390	± 117

Table 2: Table of transition energies for ^{87}Rb corresponding to Fig. 12b

3.3 Zeeman Effect

We focus on the ^{87}Rb $F = 2$ line to observe the Zeeman splitting. Zeeman splitting is most easily observed in the $1 - 3$ crossover, $2 - 3$ crossover, and $F' = 3$ lines within the $F = 2$ line. Fig. 16 shows oscilloscope traces for the Zeeman splitting for various magnetic fields strengths. We summarize our measurements below in Fig. 13. We can see that the Zeeman splitting is linear, which matches the functional form of Eqn. (3).

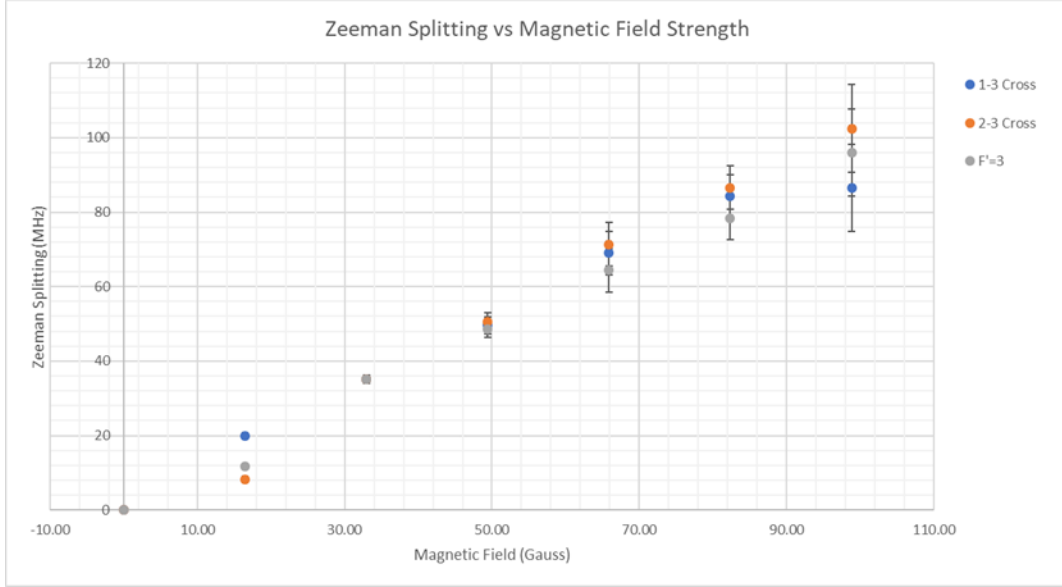


Figure 13: Zeeman splitting for the transition peaks within the $F = 2$ peak of ^{87}Rb .

$ B $ (G)	$\Delta B $ (G)	1 – 3 (MHz)	2 – 3 (MHz)	$F' = 3$ (MHz)	Δf (MHz)
0	± 0	0	0	0	± 0
16.5	± 0.330	20.0	8.19	11.7	± 0.467
33.0	± 0.330	35.1	35.1	35.1	± 1.17
49.4	± 0.330	49.6	50.5	48.7	± 2.34
65.9	± 0.330	69.0	71.4	64.4	± 5.85
82.4	± 0.330	84.2	86.6	78.4	± 5.85
98.9	± 0.330	86.6	102	95.9	± 11.7

Table 3: Data table summarizing the Zeeman splitting for the $F = 2$ peak of ^{87}Rb at various magnetic field strengths.

3.4 Landé g-factor

Using the first order approximation for Zeeman splitting, Eqn. (3), and data measured for the $F' = 3$ hyperfine transition of ^{87}Rb , we determine g_F which is summarized in Tab. 4.

f (MHz)	E (Erg)	 B (G)	g_F	Δg_F
11.7	7.75×10^{-20}	16.5	0.254	±0.0203
35.1	2.33×10^{-19}	33.0	0.381	±0.0152
48.7	3.22×10^{-19}	49.4	0.352	±0.00938
64.4	4.26×10^{-19}	65.9	0.349	±0.00689
78.4	5.19×10^{-19}	82.4	0.340	±0.00544
95.9	6.36×10^{-19}	98.9	0.347	±0.00462
Average		0.337	±0.0301	

Table 4: Table of values used to calculate g_F

4 Conclusion

4.1 Error

The calibration for the laser was performed previously and we did not have time to perform one ourselves. It appears as if our energy measurements for the hyperfine splitting are about twice too high compared to the accepted values. This could be because we used the previous calibration setting instead of performing one ourselves.

When determining the transition energies, I printed oscilloscope traces and measured frequency differences by hand, unaided by a computer program. This introduced unneeded human error into the measurements. A better alternative utilizes computer image manipulation software like ImageJ to make precise measurements digitally.

While measuring the magnetic field, it became very difficult to follow specific transition lines as the magnetic field increased. We suspect that in part, this is due to the poor quality of the oscilloscope. The trigger level was far too sensitive for fine adjustments and the oscilloscope trace was constantly fluctuating around the screen making it hard to follow specific peaks. To fix this, a higher quality oscilloscope is required.

4.2 Extensions - Need more!

Spectroscopy has many useful applications in astronomy. For planets with atmospheres that pass in front of a star, the chemical composition of the atmosphere may be determined using a spectroscopic decomposition similar to this experiment. ■

Saturated absorption spectroscopy allows signals “hidden” within a doppler-broadened peak to be resolved with fine detail. This technique can be applied measure the fine structure, and hyperfine structure constants. ■

5 Appendix

5.1 Mode Hopping

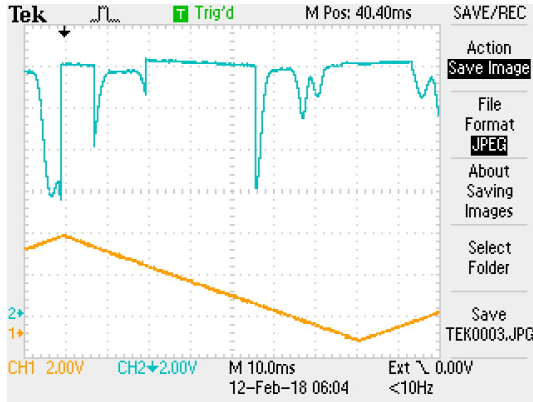


Figure 14: Rubidium spectrum with mode hopping

The series of graphs below depict mode hopping between the grating feedback and external cavity. We can see that as the relative frequency of the external cavity is increased, the laser hops to the mode with the most overlap. In graphs a-c, the laser hops through grating feedback and external cavity modes, but in d, the laser hops up to the next internal cavity mode.

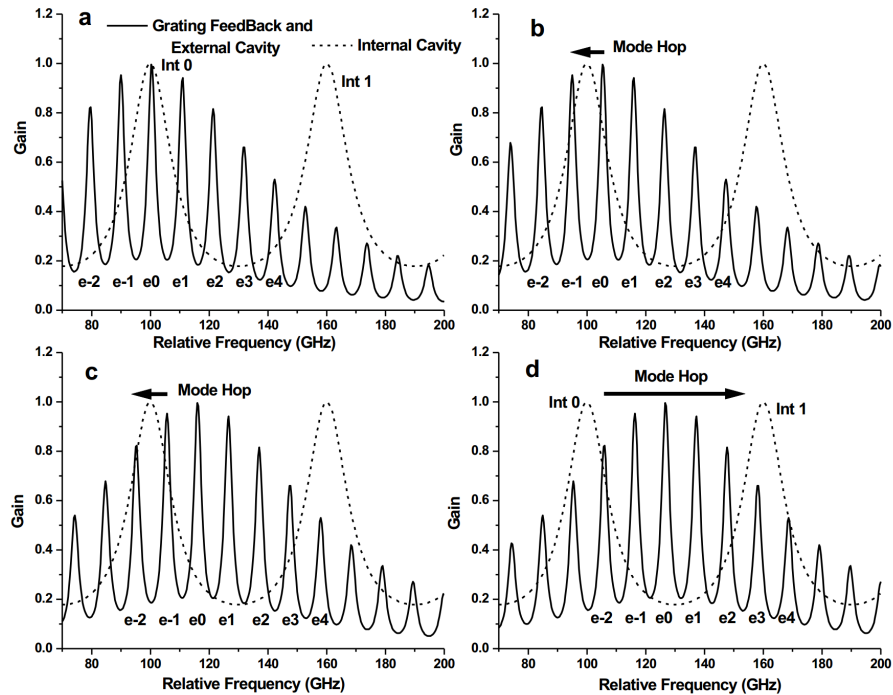


Figure 15: Depiction of mode hopping

5.2 Zeeman Splitting

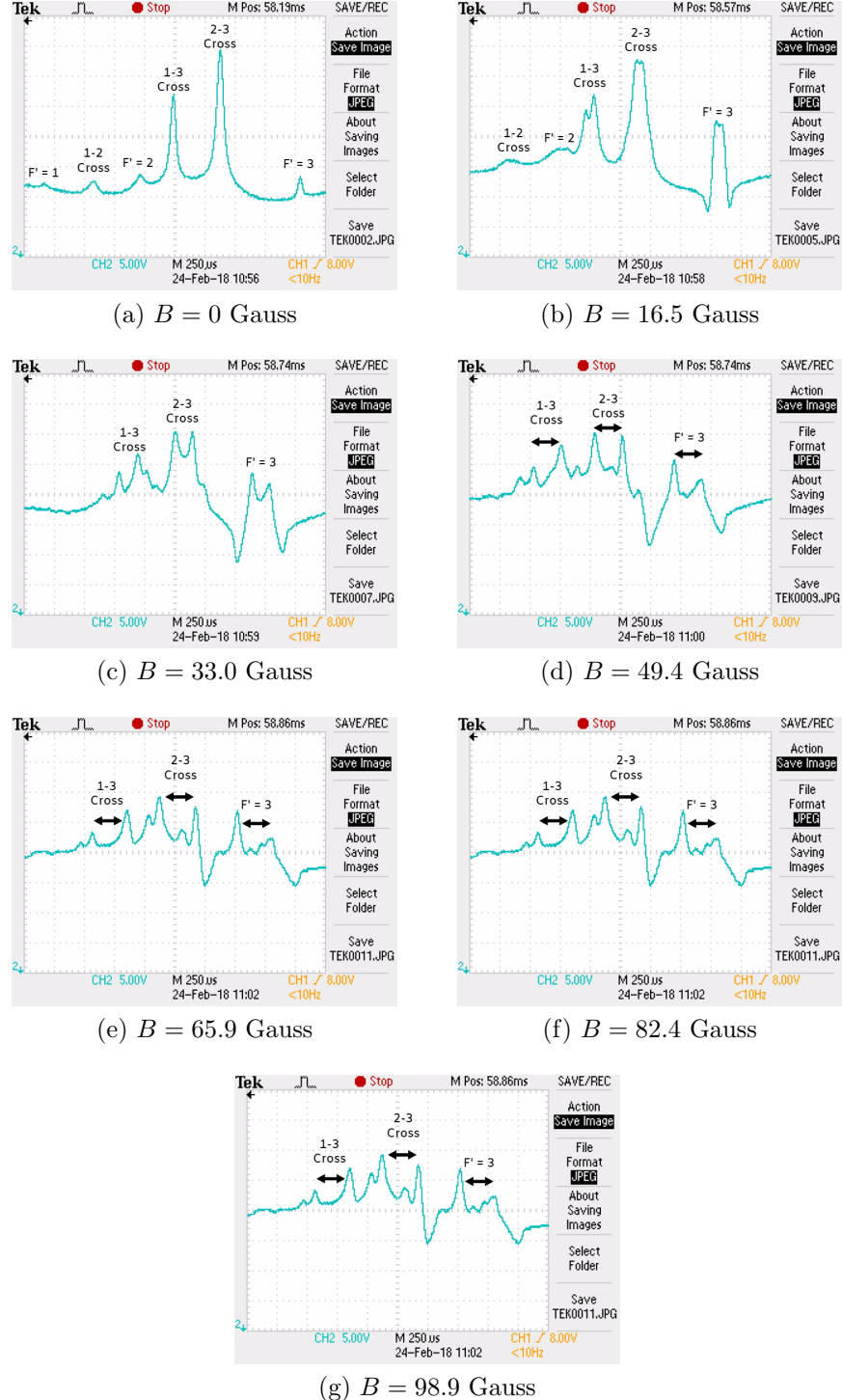


Figure 16: ^{87}Rb Zeeman splitting of the 1-3 crossover, 2-3 crossover, and $F' = 3$ state for various magnetic field strengths.

References

- [1] D. H. McIntyre, *Quantum Mechanics*. Pearson, 2012.
- [2] W. Beyermann, *Diode Laser Spectroscopy Laboratory Manual*.
- [3] D. A. Steck, *Rubidium 85 D Line Data*.
- [4] D. A. Steck, *Rubidium 87 D Line Data*.
- [5] H. Lewandowski, D. Harber, D. Whitaker, and E. A. Cornell, “Simplified system for creating a boseeinsteinkonensatz,”.